Polymer 52 (2011) 3183–3189

Contents lists available at ScienceDirect

Polymer

journal homepage: www.elsevier.com/locate/polymer

Morphological, mechanical, and electrical properties as a function of thermal bonding in electrospun nanocomposites

Sangeetha Ramaswamy [a], Laura I. Clarke [b,**], Russell E. Gorga [a,c,*]

[a] Textile Engineering, North Carolina State University, Raleigh, NC 27695, USA
[b] Physics, North Carolina State University, Raleigh, NC 27695, USA
[c] Fiber and Polymer Science, North Carolina State University, Raleigh, NC 27695, USA

ARTICLE INFO

Article history:
Received 11 March 2011
Received in revised form
6 May 2011
Accepted 13 May 2011
Available online 23 May 2011

Keywords:
Nanofibers
Carbon nanotubes
Thermal bonding

ABSTRACT

Poly lactic acid (PLA) was electrospun with various concentrations of multi-wall carbon nanotubes (MWNT) and thermal bonding was utilized as a post-processing treatment to improve the mechanical and electrical properties of the nanofibrous mats. Thermally bonded fiber–fiber junctions were observed with scanning electron microscopy. An increase in either the strength or modulus of the PLA mats both with and without MWNTs was observed; the maximum modulus and maximum strength occur at different treatment conditions. The electrical conductivity of the MWNT loaded mats showed significant improvement after treatment just below the composite melting point.

1. Introduction

Among the various methods for the synthesis of nano-fibers, electrospinning is the most popular due to its simplicity [1]. The nanofibrous nonwoven mats produced by electrospinning are expected to find major application areas in the biomedical sector (scaffolds for tissue engineering [2,3], wound healing applications [4], super absorbent media [5], and drug delivery systems [6]), in electronics (sensors [7] and fuel cells [8]), and in industrial applications (filtration fabrics [9,10] and chemical protective membranes [11]). However, one limitation of electrospun materials is their relatively poor mechanical properties, particularly the lack of cohesion between the fibers within the mat, which may lead to delamination when strained [12]. Electrospinning also enables the fabrication of nano-composite nanofibers by incorporation of nanoparticles, such as carbon nanotubes (CNTs), into the polymer solution before spinning [13,14]. Formation of such composites allows the material to be multifunctional and to serve, for instance, both a mechanical and electrical function. Polymer composites with CNTs as filler exhibit a low percolation threshold for electrical conductivity due to their high aspect ratios. Furthermore, if properly dispersed, the CNTs may significantly improve fiber (and overall mat) mechanical properties [15,16].

As mentioned above, as-spun electrospun nonwoven mats may have poor physical properties in general due to limited inter-fiber bonding and lack of molecular order in the fiber. A topic of recent interest is the development of strategies to enhance the properties of the electrospun fibers to extend their range of applications and fine tune their properties to meet the needs for specific applications [17]. Such strategies fall into two general categories: alterations in the basic spinning apparatus and methodology, or alternatively, subjecting the fibrous mats to post-processing treatments after spinning. Modifications in the electrospinning process include varying collector geometries [18], use of vibration technology [19,20], reactive electrospinning [21], use of AC voltage in the process [22], *in situ* crosslinking of fibers during electrospinning [23] and the use of different spinning environments [24]. Post-processing treatments may include selective degradation of a polymer component [25,26], surface coating [27,28] and bonding of fibers to improve fiber–fiber bonds [29–32].

Our interest lies in enhancing the properties of electrospun fibers by improving the inter-fiber bonds through thermal treatments after spinning. From an industrial perspective, such an approach would integrate naturally with existing fiber processing techniques. Previous research in this area has focused heavily on tensile strength enhancements at one processing temperature, but has not thoroughly addressed the effect on modulus, explored innately more complex composite materials, where particle dispersion and particle-polymer interactions are important, or compared the effects of different processing temperatures and

* Corresponding author at: Textile Engineering, North Carolina State University, Raleigh, NC 27695, USA. Tel.: +1 919 515 6553.
** Corresponding author. Tel.: +1 919 513 7359.
E-mail addresses: liclarke@ncsu.edu (L.I. Clarke), regorga@ncsu.edu (R.E. Gorga).

0032-3861/$ – see front matter © 2011 Elsevier Ltd. All rights reserved.
doi:10.1016/j.polymer.2011.05.023

approaches. Several studies [12,29–32] have focused on the effect of thermal bonding on mechanical properties of several different polymer systems with varying degrees of success. To summarize these previous reports, thermal bonding has been shown to improve the tensile strength of electrospun fibrous mats for each of the polymer systems. Here, we extend this work to encompass composite materials and utilize a combined, systematic approach including an analysis of the morphology, crystallinity, glass transition and melting temperatures, and mechanical and electrical properties at different doping levels and bonding conditions. We analyze the results of these varied techniques to produce a systematic understanding of how thermal bonding, with and without CNTs, affects the structure-property relationship of these nanofibers and how such treatments can be used to produce higher quality composite nanofibrous materials.

2. Experimental section

2.1. Mat fabrication

Traditional needle electrospinning from a polymer solution was utilized to generate a random mat of nanofibers as described in many reviews [1,13,33] and our previous work [2,15]. The fiber diameter can be controlled by tuning the solution viscosity (polymer concentration and molecular weight), fluid throughput, strength of the electric field, and the distance between the needle tip and collector plate (working distance) [34,35].

Poly (L-lactic acid; PLA) (Sigma–Aldrich) had a weight average molecular weight (M_w) of 73,000 g/mol. Multi-walled carbon nanotubes (MWNT) with a diameter of 15 ± 5 nm and length of 5–20 μm at 95% purity were obtained from Nano-Lab. A MWNT stock solution at a concentration of 0.1 mg/mL in dimethyl formamide (DMF) (Sigma–Aldrich) with 1% Pluronic F127 (BASF) was sonicated for 4 h in an ice bath using an Ultrasonic model 2000U generator with a needle probe operating at 25 Hz. PLA (10 wt%) was dissolved in chloroform (Sigma–Aldrich) with a DMF/chloroform ratio of 1:3. The various concentrations of MWNT used in the solutions were 0.25, 0.5, 1, 2 and 3 wt%.

The solutions were loaded into 10 mL syringes with luer-lock connections to a 4″, 20 gauge blunt tip needle. In the electrospinning process, the syringe pump (New Era Pump Systems model NE 500) was operated at a flow rate of 55 μL/min and a working distance of 15 cm with the high-voltage power supply (Glassman High Voltage model FC60R2 with a positive polarity) at 15 kV. Aluminum foil was placed over the collector plate to collect the random nonwoven mat. All samples were prepared with the same volume of solution to obtain comparable thickness. For differential scanning calorimetry (DSC), scanning electron microscopy (SEM), wide angle X-ray diffraction (WAXD) and mechanical testing, the samples were peeled off the foil. For the electrical measurements, the samples were spun on 1″ × 0.5″ glass slides.

2.2. Thermal bonding

The nonwoven mats were cut into 6 cm × 1.5 cm samples, peeled off the aluminum foil, placed in an uncovered preheated Petri dish, lined with Teflon® tape, and annealed at a range of temperatures between 70 and 175 °C in a convection oven (LR Technologies Model LN 6) for 5 min. The Teflon® tape prevented the samples from sticking to the hot Petri dish. For DSC, SEM, WAXD and mechanical tests this procedure was used and then the samples were cut into the required dimensions (defined below). For electrical measurements, the samples were spun on glass pieces and placed on the Petri dish and bonded in the oven for 5 min.

2.3. Characterization

The thermal analysis was conducted using a Perkin Elmer Diamond DSC over the temperature range of 25–200 °C with a heating rate of 30 °C/min. The glass transition, melting temperature, cold crystallization temperature, and enthalpy at melting were calculated.

The morphology of the scaffolds, before and after thermal treatment, was imaged with a Phenom SEM (FEI) operating at 5 kV. The samples were coated on a S67620 mini sputter coater (Quorun technologies) with Au–Pd at a thickness of 100 Å to reduce charging and produce a conductive surface. The SEM images were analyzed using Image J™ Software (NIH) to determine the average fiber diameter and overall porosity of the mats.

Tensile tests were performed with an Instron Model 5544 using the Bluehill™ Version 1.00 software at a crosshead speed of 10.00 mm/min. Sample gauge length was 3 cm with a width of 1.5 cm. Scaffold thickness was measured with a pair of calipers. The thickness values were confirmed using cross-sectional scanning electron microscopy (as shown in Fig. 1). The target thickness for mats in this study was 50 μm. The tensile strength and modulus were calculated by averaging ten specimens for each sample. Samples annealed at 120 °C and above experienced shrinkage. Corrections were made to account for shrinkage by zeroing the strain at the point the force deviated from the background noise, therefore ensuring all slack was taken up from the mats.

The mat void volume was calculated using Image J™ Analyzer. The SEM images obtained were converted to grayscale where different layers were made distinct. The void fraction was calculated from the area of nanofibers present (the entire area in the SEM image) in one plane (or a single layer) of the image as described previously [2,15]. The results from such analysis can be compared with an alternative approach where sample density is experimentally determined from measurements of sample volume and mass for a particular mat and compared with the expected density due to the combination of polymer, MWNT, surfactant, and air [36] to determine the porosity; similar porosity values are obtained as with the SEM analysis. It should be noted that the multi-component nature of the nanofibers (polymer, MWNT, and surfactant) complicates this alternative analysis as compared to a single component system. The mechanical properties for each sample account for the void fraction by incorporating the void volume into the cross-sectional area calculations. It is germane to

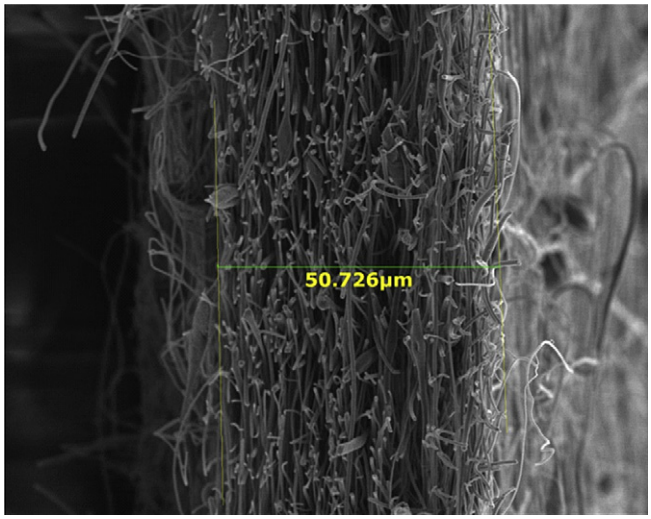

Fig. 1. Cross-sectional electron micrograph of a PLA electrospun nonwoven mat.

note that the void fraction calculated for cross-sectional SEM images and topographical SEM images was very similar (~60% for pure PLA with no heat treatment).

The Omni ATPS, XRD 1000 (Model # PH268L-25) X-ray apparatus (Cu K_α source) with a proportional counter was used for the wide angle X-ray diffraction studies. The scanning angle was from 5° to 30° with 0.1° step size.

Electrical measurements were performed with a Keithley model 6430 sub-femtoamp remote source meter in 10^{-7} torr vacuum. Flexible electrodes (copper shim, $0.25'' \times 0.5''$) were pressed against the $1'' \times 0.5''$ nanofiber-coated glass slides and secured with binder clips (Fig. 2). Plain glass without an electrospun mat served as the control, which was consistent with a PLA mat with no MWNT doping. Only samples whose current-voltage curves showed significant improvement in conductance compared to the control were included in analysis. Conductance values were obtained by fitting a line to the low voltage linear region of the current-voltage characteristic and converted to conductivity using the known electrode geometry and the measured porosity.

3. Results and discussion

To determine the glass transition (T_g) and melting (T_m) temperatures of the PLA, and thus the useful temperature range for thermal treatment, the mats were thermally analyzed using DSC. Fig. 3 shows the DSC thermograms of PLA fibers with 0 and 1% MWNT along with bulk PLA. Table 1 summarizes the melt and glass transition temperatures. These results indicate that the incorporation of MWNT in the fiber decreases T_g. It is typically expected that the addition of well dispersed nanoparticles will increase the T_g (by creating a reinforcing effect at the polymer interface), but lower T_g values have been previously reported by Logakis et al. [37]. These authors attributed the T_g decrease to the increase in free volume with the addition of the MWNT as the nanotubes are likely to prevent the packing of the polymer chains (due to the relatively large size of the MWNT and therefore a lower surface area to volume ratio). Hence, a retardation in T_g is not surprising for composites with larger nanoparticles, such as MWNT. With this increase in free volume, allowing for increased mobility of the polymer chains, the T_g decreases as the cooperative motion of the polymer chains can persist at lower temperatures. The electrospun mats exhibit a T_m that is lower than that in bulk PLA, independent of MWNT loading over this range, and due to the cold

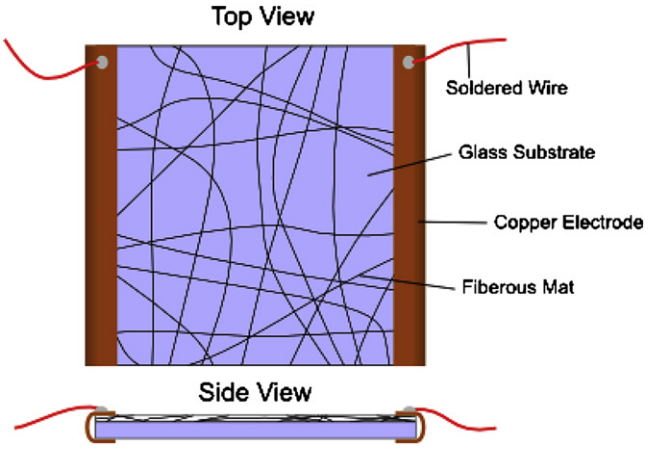

Fig. 2. A schematic of the experimental configuration for electrical measurements on the nanofibrous mats. The features of the nanofibrous mat are not to scale. Spring-loaded clips (not shown) were used to keep uniform contact between the copper electrode and the mat along the entire length of the sample.

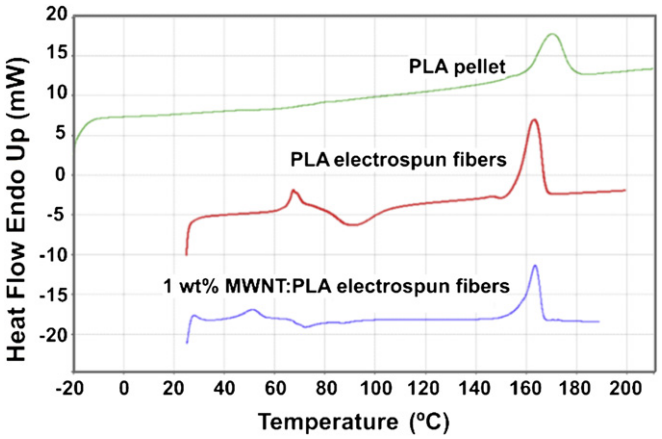

Fig. 3. DSC thermograms of the polymer pellet (as received) and electrospun samples.

crystallization in the DSC, that is, resulting when the largely amorphous electrospun PLA crystallizes during the DSC run upon heating above T_g [38]. It is germane to note that due to the presence of cold crystallization occurring during the heating run, DSC was not used to determine the crystallinity of as-spun fibers. WAXD results on crystallinity appear below.

Wide angle X-ray diffraction (WAXD) patterns for mats before and after heat treatment at 160 °C are shown in Fig. 4. No distinct crystal peaks were seen in the as-spun fibers, indicating that the lack of crystalline structure. The lack of crystal structure in the as spun mats is not surprising since it has been shown that electrospinning can prevent crystallization in semi-crystalline polymers [29]. On the other hand, when the electrospun fibers are annealed at 160 °C, a pronounced peak at about 17.5° 2θ, indicative of PLLA crystal [39], is present for samples with and without MWNT. Note that the peak amplitude varies and is in arbitrary units. This data indicates that upon heat treatment a cold crystallization process takes place when annealing just below the melt temperature (as also seen in DSC). Thus the electrospun samples are primarily amorphous and one effect of heat treatment is enhanced crystallinity when annealed in such a manner.

The temperatures chosen for thermal bonding and characterization were just above T_g (70 and 80 °C), a temperature between melting and glass transition (120 °C) and temperatures surrounding the melting temperature (150, 160 and 170 °C). The electrospun mats were annealed in a convection oven at a fixed temperature for five minutes. DSC was performed for samples heat-treated at temperatures from 70–170 °C, and shows the extent of cold crystallization as a function of MWNT concentration. Table 2 summarizes the results from the melt temperature transition, which is present in all samples but with different heats of fusion (ΔH), where the heat of fusion magnitude is related to the extent of crystallization. After treatment at 160 and 170 °C, the ΔH for the neat PLA mat is significantly higher than that for the PLA mats with 0.25 and 1 wt% MWNT and for the neat PLA mats treated at lower temperatures. Thus cold crystallization occurs for the PLA mats

Table 1
T_g and T_m obtained from DSC thermograms of the PLA pellet (as received) and electrospun samples (with and without MWNTs).

Sample	T_g (°C)	T_m (°C)	ΔH (J/g)
PLA pellet	67	170	33.7
PLA electrospun	64	163	33.1
PLA electrospun with 1 wt% MWNT	53	163	27.4

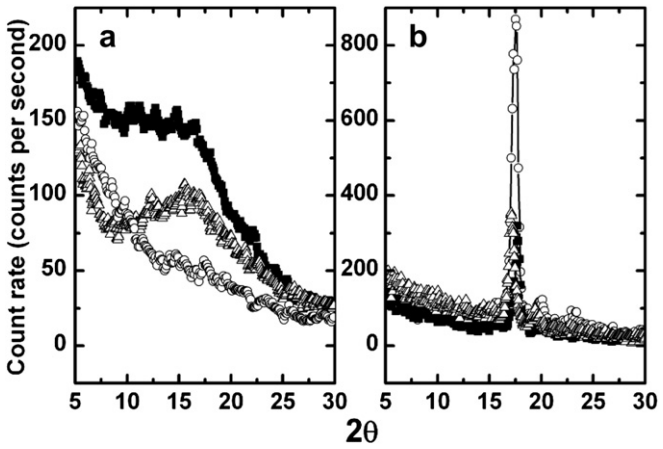

Fig. 4. WAXD spectra of PLA electrospun mats with 0 wt% (filled squares), 0.25 wt% (open triangles) and 1 wt% (open circles) MWNT as-spun (panel a) and bonded at 160 °C (panel b). Whereas no sharp features are observed in the as-spun mats, all exhibit a peak at 17.5° 2θ characteristic of crystalline PLA after heat treatment.

whereas the addition of MWNT impedes this process. This change in the extent of cold crystallization has implications for the mechanical properties, as discussed below.

Overall, the DSC and WAXD data indicates that the ideal heat treatment temperature (due to changes in the T_g and T_m) and perhaps even the dynamic reorganization processes available upon annealing (such as cold crystallization) will vary for composites in comparison with pure materials.

To determine the morphological changes of the mats as a function of thermal bonding, SEM was utilized. Fig. 5 shows the characteristic morphology for the electrospun PLA fibers, with 0 and 1 wt % MWNT loading, as a function of bonding temperature. After heat treatment at 70 °C, near the T_g, the morphology is similar to that seen in the as-spun mats (not shown) with no evident merging of overlapping fibers (fiber–fiber bonding). The lack of overt merging between overlapping fibers is characteristic of electrospun materials where the fibers are almost completely dry when deposited onto the collector. This lack of mat cohesion can negatively affect the mat's mechanical properties. When annealing at temperatures above the T_g (80 °C), relaxation of the polymer chains, which can become extended in the electrospinning process, occurs as evidenced by the tendency of the fibers to curl. Observable inter-fiber bonding is still absent. As the bonding temperature is raised to 120 °C, fiber–fiber bonds are clearly observed. At and above 120 °C, the mats visibly shrink during annealing and the annealed samples are significantly more rigid and brittle than the as-spun samples. The thermal bonding becomes more evident slightly below the melting temperature (150 and 160 °C), where the fiber–fiber junctions appear well bonded but the fibrous structure is still apparent. When the mats are treated above T_m (170 °C and higher), they melt and form a film. In general, the porosity decreases as a function of thermal bonding (Fig. 6), gradually above T_g and then dramatically above T_m. The same basic morphology changes occur in both neat and composite systems.

Table 2
Melting enthalpy (ΔH, J/g) as a function of annealing temperature for electrospun mats of PLA and PLA doped with MWNTs. The melting enthalpy of the PLA pellet is provided for reference.

Anneal temp (°C)	PLA pellet	PLA	PLA/0.25 % MWNT	PLA/ 1 % MWNT
	ΔH (J/g)			
–	33.7	33.1	31.7	27.4
70		33.0	33.6	30.0
80		33.1	33.2	35.0
120		32.3	29.5	27.1
150		35.6	35.0	39.4
160		57.2	35.4	32.0
170		54.0	26.7	30.3

Tensile tests were performed on as-spun PLA electrospun mats with MWNT loading of 0, 0.25 and 1 wt%. The tensile strength and modulus calculations account for the void volume fraction as described in the experimental section. In the as-spun mats, mechanical properties improved considerably with addition of 0.25% MWNT (Fig. 7) while the addition of 1% MWNT lowers the tensile strength and modulus. This result is consistent with previous published work on electrospun fibers loaded with MWNT [2,15]. At higher loading of MWNT (1% and above), the nanotubes are not well dispersed in the polymer matrix. These particle aggregates reduce the relative surface area and thus the amount of interfacial area available for load transfer from matrix to nanotube in addition to acting as defects (and therefore points of stress concentration) resulting in reduced strength and modulus.

Tensile strength (Fig. 7a) and modulus (Fig. 7b) were measured as a function of the thermal bonding temperature. The tensile strength improved sharply when the fibers were bonded above their T_g (70–80 °C). This is attributed to the interdiffusion of the polymer molecules at the fiber–fiber junctions due to the thermal treatment. As the bonding temperature increased, the tensile strength increased gradually as the inter-fiber junctions became more extensively bonded (as evidenced in the morphology study in Fig. 5). When the heat treatment temperature was close to the T_m (above 120 °C) another sharp increase in tensile strength was observed in the neat PLA fibers, which we attribute to cold crystallization. However, the presence of the MWNT prevents this large-scale cold crystallization (as evidenced by the DSC enthalpy data). In fact, the MWNT samples exhibit a slight decrease in tensile strength when treated near the melting temperature. This decrease could be due to relaxation of the polymer chains within the electrospun fibers, as discussed below.

The relationship between the tensile modulus and the bonding temperature is more complex. The modulus depends on the fiber–fiber interactions, fiber crystallinity, and also the effect of the thermal treatment on the relaxation of the polymer molecules, which can be elongated along the fiber axis during electrospinning. We hypothesize that when the fibers are annealed close to their T_g (70 °C) for five minutes, the heating time and temperature is not enough to create large scale motions in the bulk of the fibers, but is sufficient to cause such motions at the surface. Thus bonding occurs at fiber–fiber junctions, without significant relaxation of the polymer chains within the fibers, and the mat becomes stiffer without becoming brittle. As a result, the modulus increases considerably (except for the 0.25 wt % sample since its initial modulus is already significantly enhanced by the MWNT, indicating that bonding of fiber–fiber junctions does not further improve the reinforcing effect of the well dispersed MWNTs). This may be a useful processing point for thermal annealing. When the samples are annealed at higher temperatures, there is enough thermal energy for the polymeric chains in the bulk to relax. This causes a decrease in the modulus as the polymer chains have relaxed during heat treatment and thus are more coil-like in the heat-treated samples. On bonding the PLA nano-fibers close to their T_m, as discussed above, cold crystallization occurs and a sharp increase in modulus is obtained. However, incorporation of MWNTs in the sample prevents significant cold crystallization for samples annealed at 160 °C and above (as indicated by the DSC data) and therefore the modulus continues to drop for samples loaded with MWNT as the chains become further disordered. This effect also decreases the tensile strength of the fibers in analogous manner, in

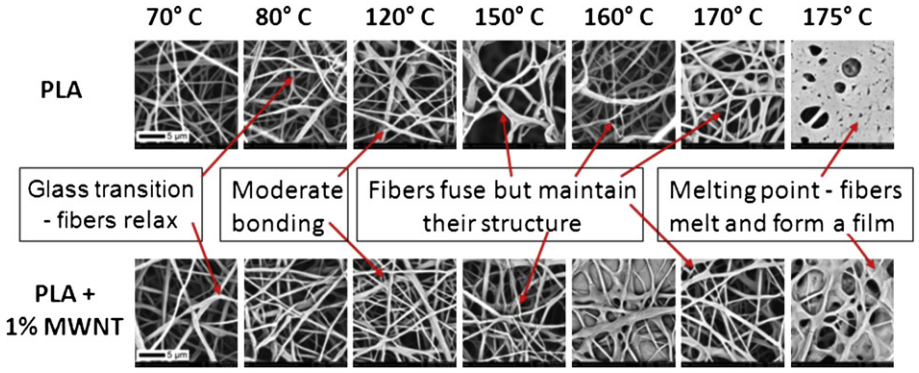

Fig. 5. Electron micrographs of PLA and PLA/1% MWNT nanofiber morphology as a function of bonding temperature. The scale of each image is identical; the scale bar is 5 μm. The average fiber diameter for each sample is approximately 400 nm.

that the strength of aligned polymer chains is higher than that after the chains have relaxed to a coil-like state. Thus, in the tensile strength measurements for MWNT-doped samples (discussed in the previous paragraph), at temperatures above T_g chains are becoming disordered (tending to decrease the tensile strength); however, this effect is counteracted by effect of increased fiber–fiber contacts.

In summary, for neat PLA mats, thermal treatment near T_m, which significantly increases the crystallinity within the fibers, provides the best mechanical properties (highest strength and highest modulus); however most of the fibrous morphology is lost and the sample is predominantly film-like. Treatment at the highest temperature conditions that still maintains the fiber morphology required for a particular application provides the best results for PLA mats, because cold crystallization enhances the mechanical properties. For PLA-MWNT samples, dispersion of MWNT dopant is important, and moderate doping (0.25 wt% MWNT:PLA) showed better results than higher doping levels (1 wt % MWNT:PLA), which is consistent with a previous report [40]. Treatment above T_g but below T_m (~120 °C), results in bonding between fibers, which maximizes mat tensile strength. On the other hand, the maximum modulus occurs at a lower temperature, near the T_g, where some bonding occurs between fibers but the polymer chains within the fibers do not yet relax.

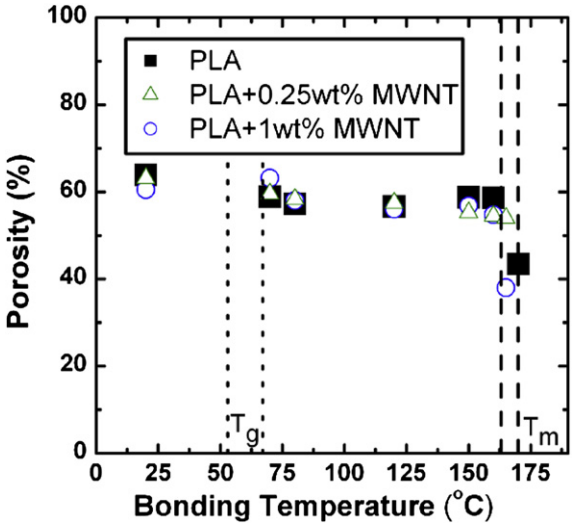

Fig. 6. Porosity (as calculated from electron micrographs) as a function of bonding temperature. The T_g and T_m regions indicate the range of observed T_g and T_m values for different sample types.

Polymer composites with MWNT filler exhibit a low percolation threshold for electrical conductivity owing to their large aspect ratios [41–43]. In nanofibrous composites the conductivity depends not only on the concentration of the filler but also on the morphology of the fiber as well as that of the resultant nonwoven mat. Our previous experimental [2,15,40] and computational research [42] suggests that current within composite nanofibrous materials may flow through pathways consisting of short segments of many different fibers, rather than through a series of nanotubes within a single fiber [42]; therefore, the fiber–fiber junctions play an important role in the resultant conductivity. When such an electrospun mat is thermally annealed and the connectivity of the fiber–fiber network increases, the conductivity will be affected in two ways. First, the number of fiber–fiber junctions will increase thus creating additional possible pathways for the current flow. This effect could lower the percolation threshold and/or raise the conductivity. Second, the resistance at each junction will be reduced, thus improving the overall conductivity.

Electrical measurements were performed on as-spun and annealed PLA nano-fibers loaded with 0.5, 1, 2 and 3 wt% MWNT after treatment at different bonding temperatures (Fig. 8). While conductivity measurements were taken for all nanotube concentrations under all annealing temperatures, only the data from samples that displayed a distinct difference from the background measurement were included in Fig. 8. Thus, the absence of data at any temperature corresponds to very low conductivity (*i.e.* not statistically different from the background). At this long (1″) length scale, conductivity values are low but observable. Following the data for 2 wt% MWNT loading, the conductivity is constant until just below the melting temperature, where it dramatically increases (by >30×). Here, the MWNT may have some ability to slightly reorient within the fibers, enabling better nanotube-nanotube contacts along the current carrying pathways. When heat treating above T_m, the samples form films and the conductivity decreases. Upon melting, the existing nanotube network, which is supported by the fiber structure, is likely partially disrupted as the polymer flows (moving with it MWNT) and thus the conductivity decreases. Furthermore, interactions between MWNT, which may occur in the melted state and lead to additional aggregation, will also detrimentally affect conductivity.

As the loading of MWNT is lowered to 0.5 and 1 wt%, the conductivity of the as-spun samples decreases as expected. For the 1 wt% sample, the conductivity is below our resolution for the as-spun mat, but observable after heat treating near T_g and above indicating that the increase in fiber–fiber bonding increases the conductivity at this doping level. Conductivity again increases dramatically when treated just below T_m. Interestingly, the 1 wt and 2 wt% samples exhibit similar conductivity values after

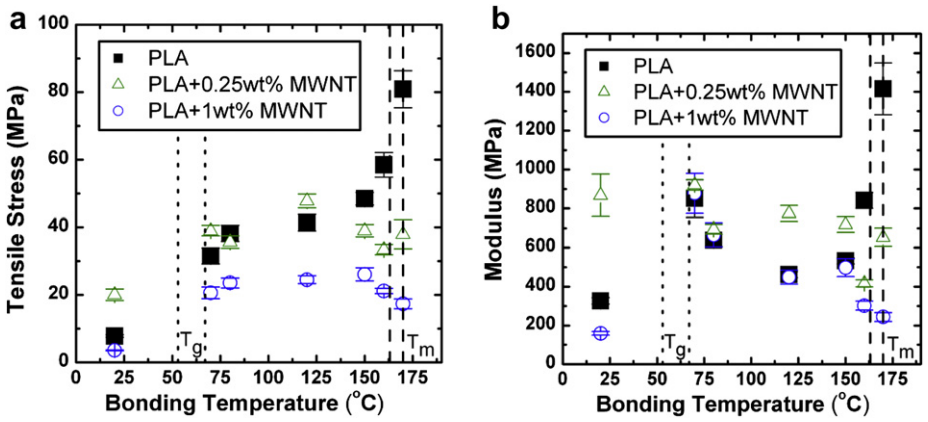

Fig. 7. (a) Tensile Strength and (b) Tensile modulus as a function of bonding temperature for PLA (filled squares), PLA-0.25 wt % MWNT (open triangles) and PLA-1 wt % MWNT (open circles). The T_g and T_m regions indicate the range of observed T_g and T_m values for different sample types.

annealing at any temperature above T_g. Thus, improving mat continuity by thermal treatment may be a better way to achieve enhanced conductivity than increasing the amount of dopant. At 0.5 wt% doping, conductivity was only observable when heat treating just below T_m (that is, after the most beneficial heat treating); the conductivity value at this point was significantly lower than the 1 wt% and 2 wt% samples heat treated in the same manner. Increasing the doping density to 3 wt% did not improve the conductivity in as-spun or heat treated mats; in fact, the results for 3 wt% are similar to that of the 0.5 wt%. Aggregation of the MWNT (in the as-spun samples) at such a high doping level is a likely explanation for this effect. Overall these results indicate that enhanced conductivity can be obtained with lower doping density if thermal treatment is utilized; thus, aggregation effects can be minimized by doping at an optimal level (in our case around 1 wt%) and then improving the nanotube–nanotube contacts (via heat treatment) to increase conductivity. For instance, when heat treating at 160 °C, the conductivity for the 1 wt% sample is similar to that of the 2 wt% sample, ~30 × higher than the 0.5 wt% and 3.0 wt% samples, and ~ 300 × higher than without heat treatment.

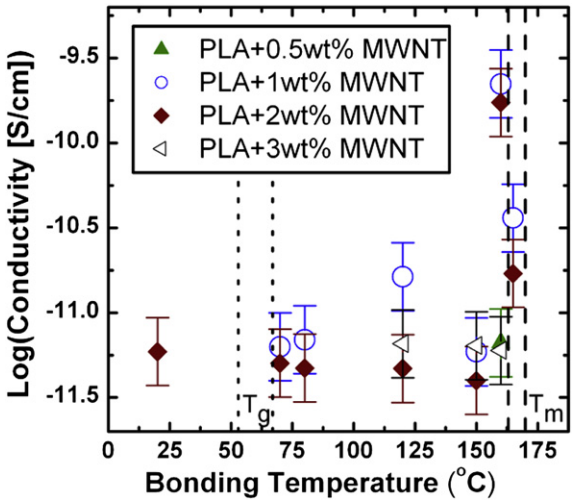

Fig. 8. Log conductivity as a function of bonding temperature at MWNT concentrations of 0.5 (filled triangle), 1 (open circle), 2 (diamond), and 3 (open side triangle) wt %. The T_g and T_m regions indicate the range of observed T_g and T_m values for different sample types. The conductivity values take into account an average porosity at each bonding temperature.

4. Conclusions

Thermal bonding was used as a post-processing treatment to improve the mechanical and electrical properties of MWNT-doped and neat electrospun nanofibrous PLA materials. SEM imaging confirmed the improvement in inter-fiber connection with thermal treatment, which was associated with an increase in strength. The maximum strength (tensile strength) for MWNT:PLA mats occurred for bonding between T_g and T_m. The maximum modulus occurred at lower bonding temperatures (near T_g) as the fiber–fiber contacts became fused. In contrast, the modulus dropped at higher bonding temperatures as the internal molecular structure relaxed. Cold crystallization was seen in the neat PLA nanofibrous mats when annealed near T_m, which resulted in a sharp increase in tensile strength as well as modulus. This cold crystallization was impeded for MWNT doped mats as shown by DSC. Thus for composite mats, the heat treatment temperature for maximum mechanical properties differs from that for neat PLA. Electrical measurements showed an increase in conductivity when heat treating near T_g, another significant increase just below T_m, and a relative insensitivity to treatment between these steps. Therefore, the thermal relaxation mechanism that negatively impacts the tensile properties has a strong positive effect on the electrical properties (due to the resulting rearrangement of the MWNTs). Specifically, after heat treating just below T_m, 1 wt % MWNT samples showed similar conductivity to those doped with 2 wt % MWNT and much higher values than samples with higher or lower MWNT doping. Thus, once a sufficient minimal level of well-dispersed MWNT is present, heat treating can enable significant conductivity enhancements and could be utilized as an alternative to increasing doping density.

Acknowledgment

The authors wish to thank Nagarajan TM, Judy Elson, Torissa Hoffman, Jiaxing Bao, Nagarajan Thoppey Muthuraman, and Erik Skau for laboratory assistance. The authors also thank the NC State University Department of Textile Engineering, Chemistry, and Science for financial support for Sangeetha Ramaswamy.

References

[1] Andrady AL. Science and technology of polymer nanofibers. Hoboken, NJ: Wiley; 2008.
[2] McCullen SD, Stevens DR, Roberts WA, Clarke LI, Bernacki SH, Gorga RE, et al. Int J Nanomed 2007;2:253–63.
[3] Ma Z, He W, Yong T, Ramakrishna S. Tissue Eng 2005;7-8:1149–58.

[4] Park KE, Jung SY, Lee SJ, Min BM, Park WH. Int J Biol Macromol 2006;3-5: 165–73.
[5] Carr ME. Storming media; Annual report-1, 2003, 3, 1–24.
[6] Zeng J, Xu X, Chen X, Liang Q, Bian X, Yang L, et al. Control Release 2003;3: 227–31.
[7] Bishop A, Gouma P. Rev Adv Mater Sci 2005;10:209–14.
[8] Kim C, Park SH, Lee WJ, Yang KS. Electrochim Acta 2004;2-3:877–81.
[9] Graham K, Ouyang M, Raether T, Grafe T, McDonald B, Knauf P. Polymeric nanofibers in air filtration applications. In: Proceedings of the fifteen annual technical conference and expo of the American filtration and separations society, Galveston, Texas; 2002.
[10] Filatov Y, Budyka A, Kirichenko V. Electrospinning of micro-and nanofibers: fundamentals and applications in separation and filtration processes. New York: Begell House; 2007.
[11] Ramaseshan R, Sundarrajan S, Liu Y, Barhate R, Lala NL, Ramakrishna S. Nanotechnology 2006;12:2947–53.
[12] You Y, Won Lee S, Jin Lee S, Park WH. Mater Lett 2006;11:1331–3.
[13] Gogotsi Y. Nanotubes and nanofibers. Boca Raton, Fl: CRC, Taylor & Francis; 2006.
[14] Ko F, Gogotsi Y, Ali A, Naguib N, Ye H, Yang G, et al. Adv Mater 2003;14:1161–5.
[15] McCullen SD, Stevens DR, Roberts WA, Ojha SS, Clarke LI, Gorga RE. Macromolecules 2007;40:997–1003.
[16] Moniruzzaman M, Winey KI. Macromolecules 2006;16:5194–205.
[17] Tan S, Huang X, Wu B. Polym Int 2007;56(11):1330–9.
[18] Li D, Ouyang G, McCann JT, Xia Y. Nano Lett 2005;5:913–6.
[19] He JH, Wan YQ, Yu JY. Int J Nonlinear Sci Numer Simulat 2004;5:253–62.
[20] Wan YQ, He JH, Yu JY. Polym Int 2007;11:1367–70.
[21] Ji Y, Ghosh K, Li B, Sokolov JC, Clark R, Rafailovich MH. Macromol Biosci 2006; 10:811–7.
[22] Kessick R, Fenn J, Tepper G. Polymer 2004;9:2981–4.
[23] Gupta P, Trenor SR, Long TE, Wilkes GL. Macromolecules 2004;24:9211–8.
[24] Teo W, Ramakrishna S. Nanotechnology 2006;14:89–106.
[25] You Y, Youk JH, Lee SW, Min BM, Lee SJ, Park WH. Mater Lett 2006;6:757–60.
[26] Han SO, Son WK, Cho D, Youk JH, Park WH. Polym Degrad Stab 2004;2: 257–62.
[27] Rubner MF, Rutledge GC. Adv Mater 2007;19(2):255–9.
[28] Ma M, Mao Y, Gupta M, Gleason KK, Rutledge GC. Macromolecules 2005;23: 9742–8.
[29] Zong X, Ran S, Fang D, Hsiao BS, Chu B. Polymer 2003;17:4959–67.
[30] Choi SS, Lee SG, Joo CW, Im SS, Kim SHJ. Mater Sci 2004;4:1511–3.
[31] Choi SS, Lee YS, Joo CW, Lee SG, Park JK, Han KS. Electrochim Acta 2004;2-3: 339–43.
[32] Lee SJ, Oh SH, Liu J, Soker S, Atala A, Yoo JJ. Biomaterials 2008;10:1422–30.
[33] Doshi J, Reneker DHJ. Electrostatics 1995;2:151–60.
[34] Zong X, Kim K, Fang D, Ran S, Hsiao BS, Chu B. Polymer 2002;16:4403–12.
[35] Deitzel J, Kleinmeyer J, Harris D, Beck Tan N. Polymer 2001;1:261–72.
[36] Zong X, Ran S, Kim K-S, Fang D, Hsiao B, Chu B. Biomacromolecules 2003;4: 416–23.
[37] Logakis E, Pandis C, Peoglos V, Pissis P, Stergiou C, Pionteck J, et al. J Polym Sci B Polym Phys 2009;8:764–74.
[38] Ali F, Chang YW, Kang SC, Yoon JY. Polym Bull 2009;1:91–8.
[39] Zhang R, Ma PXJ. Biomed Mater Res 1999;4:285–93.
[40] McCullen SD, Stano KL, Stevens DR, Roberts WA, Monteiro-Riviere N, Clarke LI, et al. J Appl Polym Sci 2007;105:1668–78.
[41] Stauffer D, Aharony A. Introduction to percolation theory. CRC Press; 1994.
[42] Stevens DR, Downen LN, Clarke LI. Phys Rev B 2008;78:235425–9.
[43] Bauhofer W, Kovacs JZ. Compos Sci Technol 2008;69(10):1486–98.